JET–R(97)09

Theoretical and Experimental Simulation of Accident Scenarios of the JET Cryogenic Components

Part I: The JET In-vessel Cryopump

P A Ageladarakis, N P O'Dowd[1], S Papastergiou,
and G A Webster[1].

JET Joint Undertaking, Abingdon, Oxfordshire, OX14 3EA, UK.
[1] Imperial College, Exhibition Road, SW7 2BX, London, UK.

Preprint of paper submitted for publication in IMECHE
– Journal of Mechanical Engineering Science

October 1997

Abstract:

A large cryopump has been operational since 1994 inside the plasma chamber of JET (Joint European Torus), the world's largest thermonuclear fusion facility. In this work, an analytical model, which analyses the uncontrolled warm-up behaviour of the cryopump and associated water cooled components, under all possible operating conditions, is presented. The system behaviour is simulated for a wide range of fault conditions, e.g. loss of vacuum, loss of cryogen flow, loss of cooling water supply and combinations of these. The model is validated by a series of experiments conducted both in a specially designed test rig and inside the JET vacuum vessel, using real scale components. Based on this analysis, an automatic safety system has been constructed and implemented into the JET operation routines. The system incorporates protective actions (e.g. draining) which prevent the development of excessive stresses in the cryopump components, thus ensuring their mechanical integrity and reliability. The work has been divided into two parts, Part I outlines the model used in the analysis and examines the behaviour of the divertor cryopump; Part II deals with a different type of cryopump which operates outside the plasma chamber.

Keywords: JET Tokamak, nuclear fusion, safety, cryopump, modelling

NOTATION

A	surface area
C_p	specific heat of mass at constant pressure
C_p'	specific heat of coolant at constant pressure
C_{ij}	radiation exchange coefficient
dT	temperature change of a mass over the incremental time dt
dT'	temperature change of a coolant over the incremental time dt
h_a	convection coefficient of a torus fluid
$\sum W$	net heat flux from the surroundings
KA	overall heat exchanger coefficient
m	mass
$\dot{m}$	coolant mass flow rate
s	conduction path
t	time
T	temperature
T_f	temperature of a fluid surrounding a component in case of a vacuum loss
T'_n	fluid inlet temperature
T'_{out}	fluid outlet temperature over the time step Δt

$T_i(t)$, $T_i(t+\Delta t)$ temperature of ith component at times t, $t+\Delta t$ respectively

$\Delta\theta_m$ mean temperature difference in a heat exchanger

Δt time step

ε emissivity

λ thermal conductivity

φ view factor

σ Stefan - Boltzmann constant

Suffixes

i component *i*

j 1,2,3,... different masses or components which interact with i^{th} component

Abbreviations

GDC Glow Discharge Cleaning

GN Gaseous Nitrogen

JET Joint European Torus

LN Liquid Nitrogen

MK1,2 Mark 1,2 Divertor

ScHe Supercritical Helium

1 INTRODUCTION

Fusion is a nuclear reaction where nuclei from light atoms (such as hydrogen) merge to form heavier ones (such as helium) releasing extremely large amounts of energy (**1**). The application of controlled fusion, for the purpose of power generation, has been explored using two different approaches, the inertial and the magnetic-confinement method. The former uses powerful laser beams which bombard solid pellets of extremely dense nuclear fusion fuel. The pellets warm up rapidly and explode producing the desired energy. The magnetic-confinement method, utilises the principle that charged particles can be controlled by magnetic fields. The fusion mixture is heated to extremely high temperatures (on the order of 10^8 degrees) and transforms into a plasma state, i.e. a mixture of positively charged nuclei and free negatively charged electrons. Powerful magnets force the plasma particles to travel along magnetic lines, inside a chamber, causing numerous collisions and producing large amounts of energy. One of the most efficient magnetic confinement devices is the so called Tokamak (**2**) which comprises a toroidal plasma chamber.

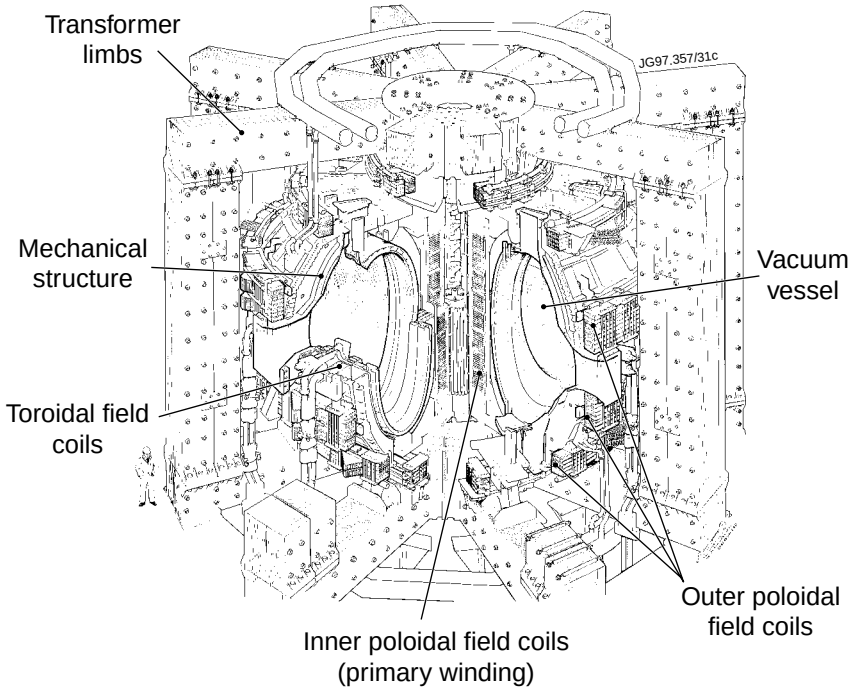

Figure 1. The JET Apparatus

The JET machine, illustrated in Fig. 1, is the world's largest and perhaps most successful Tokamak. Its overall height and diameter are 12 and 15m respectively, with a toroidal-shaped vacuum vessel, 4.1 m high and 2.6 m wide, and a major radius of 2.96 m. In 1994, JET produced the first significant (MW scale) fusion power from a Deuterium -Tritium (DT) plasma, producing 1.7 MW for 2secs, a landmark in the area of fusion science (**3**).

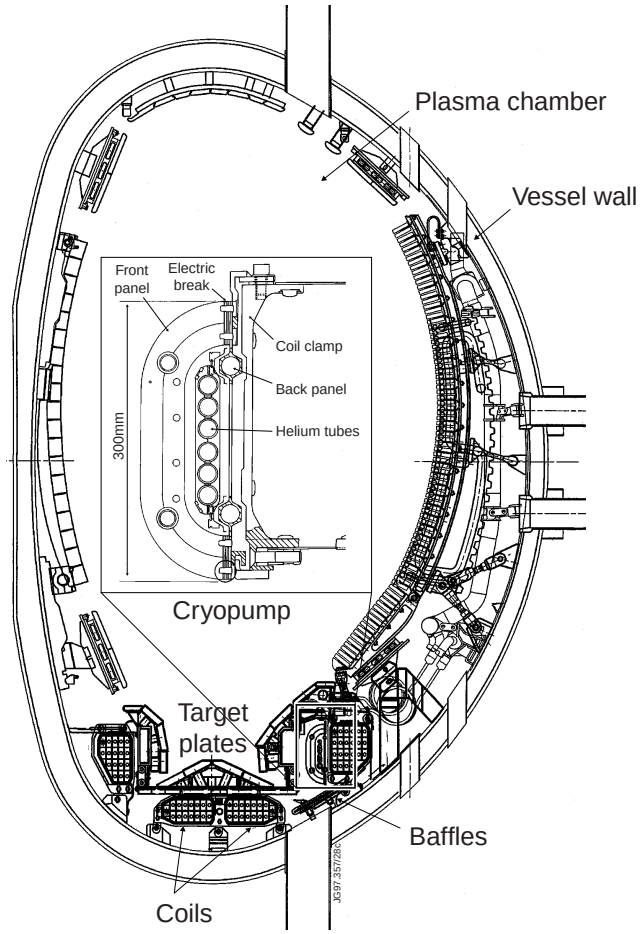

Figure 2 Cross section of the JET Tokamak with the MK1 Divertor configuration (post 1993).

The efficiency of existing Tokamaks (including JET) is limited by the influx of impurities from the vessel wall into the plasma. To alleviate this problem, the JET machine was altered in 1992-4, and a number of components were installed inside the plasma chamber, forming the so called Pumped Divertor, (**4)**. One of the main components of the JET Divertor configuration, illustrated in Fig. 2, is a large cryogenic pump (see insert in Fig. 2) which controls the density of the plasma in the divertor region and the impurity influx from the vessel walls. Since its installation, the divertor has enhanced the performance of the JET machine by contributing to longer (up to 20 sec) cleaner (fewer impurities) and more stationary H-mode plasmas (**5**), (**6**).

2 THE DIVERTOR CRYOPUMP

The cryopump is a key element of the JET divertor configuration. It has a pumping speed of 500 000 lt/sec for deuterium at 300K. The pump, a section of which is shown in Fig. 3, consists of two independent 180^{o} half circular assemblies which form a ring 20m long and 0.3m high. Each assembly incorporates a cryocondensation surface, cooled by supercritical helium (ScHe),

at 2.7 bar and 4.3 K. This surface, which is the coldest region inside the JET vacuum vessel, is surrounded by two different screens which are cooled by a forced flow of liquid nitrogen (LN), at 4 bar and 77K. The two cryo-shields are mounted together via ceramic brakes and they are cooled in series. The rear shield is constructed from a low emissivity highly polished stainless steel while the front one is a high emissivity, black coated chevron type panel, made from Siclanic (CuNiSi) ((**7**), (**8**)).

The difference in thermal properties of the two LN screens produces dissimilar warm-up or cool-down rates which may lead to significant temperature gradients. According to the design and manufacturing specifications the (global) temperature gradients between the front and back panels must never exceed 150^{o}C (**9**).

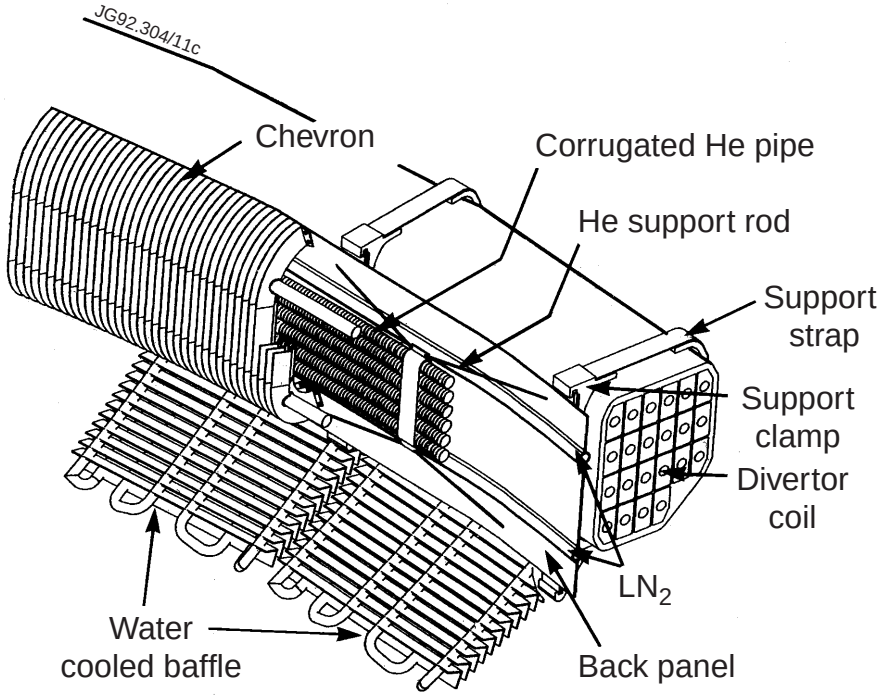

Figure 3. A Three Dimensional View of the JET Divertor Cryopump.

The whole cryopump assembly is attached (along its toroidal length) to a magnetic coil via ceramic (Al_2O_3) pads, with 48 equidistant stainless steel clamps. Elsewhere, the pump is thermally protected from the relatively warm coil by the intersection of 11 thin stainless steel radiation shields. As seen in Fig. 3, the pump is additionally protected from the hot vacuum vessel wall by water-cooled baffles, made also from Siclanic, while screening from the extremely hot plasma is provided by the water-cooled target plates, see Fig. 2. Figure 4(a) depicts the first divertor configuration (called MK1) which was installed in 1994 (**4**). In late 1995, a different set of target plates was installed (MK2) as part of the JET experimental program (see Fig. 4b). The effect of the target plate configuration on the behaviour of the cryopump was also examined in the analysis.

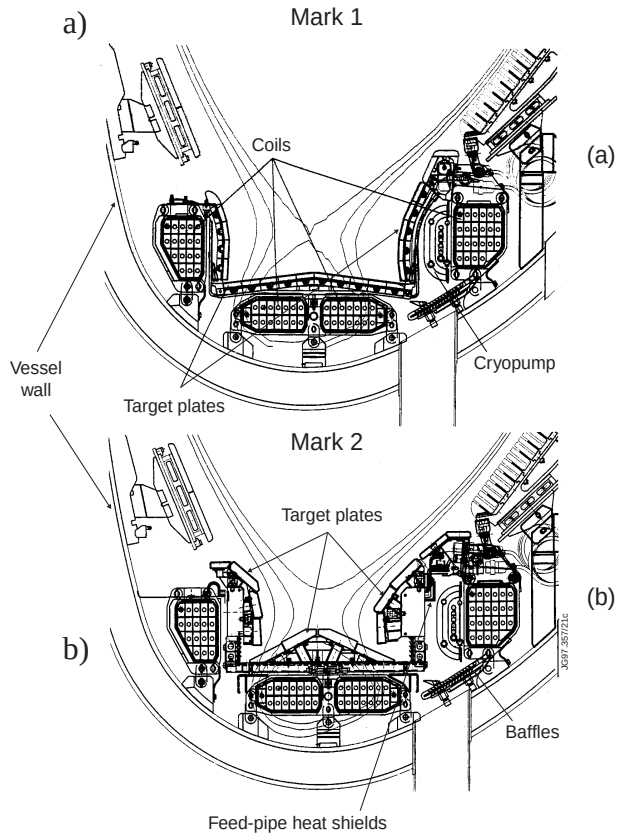

Figure 4. (a) The MK1 Divertor (post 1993), (b) The MK2 Divertor (post 1995).

3 OPERATING MODES.

The JET Tokamak and the in-vessel cryopump undergo a series of different operating modes on a routine basis such as baking, glow discharge cleaning (GDC), machine restart and normal operation. The cryopump is also designed to withstand forced warm-ups, as well as regenerations (daily or weekly for the helium loop with tritium or deuterium plasmas respectively, and at the end of each experimental campaign for the nitrogen loop). The regeneration of the helium panels is performed well before the explosive limit (i.e., 15 mbar of a hydrogenic gas) or the saturation level. Normal operation is considered to be the situation when the torus vacuum is good and all coolants (water, cryogens and freon) are flowing in the circuits. Throughout the present analysis "good vacuum conditions" means pressure lower than 10^{-3} mbar, while "bad vacuum" implies pressures higher than 10^{-3} mbar. Baking is a cleaning process in which the vacuum vessel is heated up to 350^{o}C under constant pumping (vacuum), and is used for the desorption of gases entrapped in the microstructure of the vessel walls. GDC is also a cleaning process, which removes tightly entrapped impurities either by chemical reactions or by induced desorption (**10**).

The Restart of the machine follows baking and GDC and occurs after shut downs or complete draining of the in-vessel cooling systems. During this mode, coolants are (re)-introduced inside the relevant systems under good vacuum conditions. Restart here is defined as the condition when there is no water in the system.

Finally Regeneration is the process of deliberate stoppage of cryogen flow, which allows the removal of cryo-condensed particles by conventional pumps, in order to reinstate the pumping capability of the saturated cryopump walls.

4 ABNORMAL EVENTS AND RISKS ON THE CRYOPUMP

Any deviation from the previously described conditions may be characterised as abnormal. The components must be protected against such events, and be able to withstand resulting forces or heat fluxes. The accidents which are considered here are: Loss of water flow in the baffles and/ or target plates; loss of cryogen flow (i.e., ScHe, and LN); loss of torus vacuum by the inleak of different gases and at different pressures (from a few mbar to 1 bar), and all possible combinations of the above. These off-normal events are assumed to take place during all the operating Tokamak modes in JET.

Finite element analysis (**9**) has shown that if the temperature difference (ΔTs) between the front and back LN panels exceeds 150^{o}C, yielding can occur in the area between the chevrons and the cooling pipes. This is due to bending stresses caused by the different expansion of the LN panels. It should be pointed out that even if localised yielding occurs, it was found in (**9**) that only a small number (less than 2%) of chevrons, located at either side of the cryopump subsections, are subjected to these high stresses, while the stresses in the rest of the structure remain elastic. Nevertheless, the stringent quality and reliability standards of JET cannot tolerate any failures, since a repair session would cause a general shut-down and an in-vessel intervention. Therefore, the requirement that the temperature differences between the front and back LN panels remain less than 150^{o}C is enforced. The present analysis deals with the evaluation of scenarios which may lead to high temperature gradients and in such cases suggest protective actions within specific time scales to avoid such a development.

5 BOUNDARY CONDITIONS AND ASSUMPTIONS

The boundary conditions of the problem can be summarised as follows: Torus temperature: varies between 20^{o}C and 350^{o}C (maximum temperature during baking). This is the temperature of the remote environment and is an input to the model.

Target plates: the MK1 Target plates (Fig. 4a) consist of water-cooled stainless steel armours and of beryllium or graphite tiles facing the plasma (different tile materials were examined to evaluate the effect on the plasma performance (**4**)). When water is flowing in these components their temperature is taken to be 20^{o}C. The temperature of the tiles depends on the vessel temperature, the plasma pulses, and on the contact between them and the supporting water cooled armours (**8**).

Baffles: similarly, with water flowing in the baffles the average temperature is considered to be 20^{o}C.

If there is no water flowing in the above systems their temperature is determined from the analysis assuming steady state conditions.

The Divertor Coil: is constructed from a copper core constantly cooled by freon and wrapped with impregnated epoxy glass. The whole structure is enclosed in a stainless steel metallic casing. The temperature of the copper remains at ~20^{o}C, except during plasma pulses when it reaches 80^{o}C in 20 sec and drops to its initial level in 30 min.

Cryopump: with cryogens flowing, the LN screens are assumed to remain at 77K, while the ScHe panel remains at 4.3 K. Thus there is no significant temperature gradient along the toroidal pipework, as indeed shown from continuous temperature measurements by the JET control and data acquisition systems.

Torus inleak: The medium which breaches the torus vacuum is considered to be in the gaseous state and in cases of air inleaks, the air is assumed to be without vapour (dry air). In addition, it is assumed that the gas is in uniform contact with the components of concern, and that at the time of contact the medium reaches the vessel temperature.

Plasma: in this analysis the effect of the plasma is ignored since during an accident (e.g., loss of vacuum) the plasma extinguishes almost instantly (**11**), (**12**) and does not significantly affect the behaviour of the pump (the warm-up time constants are 2-4 orders of magnitude slower). The steady state behaviour of the pump under plasma operation was thoroughly examined during the design phase (**13**). Furthermore, eddy currents due to plasma disruptions and resultant stresses have also been analysed in detail (**14**), (**15**).

6 THE MODEL

The thermal histories of the cryopump components were calculated by a flexible code able to perform steady state and transient analyses. Similar modelling techniques have been used for

theoretical studies regarding various first wall components of fusion reactors (**16**), (**17**), (**18**). Thermal analyses of pressurised water fission reactors have also been conducted using this type of model (**19**), (**20**).

The computer code takes into account the following components: the cryopump, the divertor coil with its 11 radiation shields, the target plates and target shields, the baffles and the vacuum vessel. It deals with the as-made geometry of the whole assembly, the vacuum conditions and the coolant flow conditions for each component.

The heat balance for every component involved is given by the following equation:

$$m_i Cp_i \frac{dT_i}{dt} = \pm \sum W_i - \dot{m} \int Cp' dT' \qquad (1)$$

where ,

m_i = mass of the i^{th} component

C_{pi} = specific heat of i^{th} component

dT_i = temperature change of component i over the incremental time dt

t = time

$\sum W_i$ = net heat flux to the i^{th} component from the surroundings

m = coolant mass flow rate

$C_p{}^{l}$ = specific heat of coolant

dT^{l} = temperature change of the coolant over the incremental time dt

The aim of the analysis is to calculate the temperature of component, i, at any time, t. With known heat fluxes and coolant temperatures, the above equation can be easily solved. However, if the outlet coolant temperature is unknown (as in most cases), an additional equation must be used. The second equation can be derived by regarding the component i as a heat exchanger and therefore,

$$m\, C_p{}^{l}\, dT^{l} = KA\, \Delta\theta_m \qquad (2)$$

with,

KA = overall heat exchanger coefficient which quantifies the thermal resistance along the heat path

$\Delta\theta_m$ = mean temperature difference of a heat exchanger

The mathematical formulation of the term $\sum W_i$ in Eq. (1) is given by:

$$\sum W_i = \sum\{ \varphi_{ij} C_{ij} A_i (T_i^4 - T_j^4) + h_a A_i (T_i - T_f) + \frac{\lambda_j A_j (T_j - T_i)}{s_{ji}} \quad (3)$$

where,

φ_{ij} = view factor between *i* and *j* components

C_{ij} = radiation exchange coefficient

$A_{i,j}$ = surface area of of components *i* and *j* respectively

$T_{i,j}$ = temperature of components *i* and *j* respectively

h_a = convection coefficient of a torus fluid

T_f = temperature of fluid surrounding i^{th} component

λ_j = thermal conductivity of mass *j*

s_{ji} = conduction distance between *i* and *j* components

The radiation exchange coefficient is determined from

$$C_{ij} = \varepsilon_i \varepsilon_j \sigma \quad (4)$$

where,

$\varepsilon_{i,j}$ = emissivity of mass *i* and *j*

σ = Stefan - Boltzmann constant

Equation (3) indicates that three modes of heat transfer are taken into account. The first term on the RHS of Eq. (3) represents the radiation heat exchange, while the second and third parts represent the convective and conductive heat transfer respectively. Molecular conduction, or rarefied gas heating (non-viscous flow) are not significant for the examined pressure ranges, as will be shown later.

The evaluation of the view factors φ_{ij} was carried out by means of the Hottel's Cross String method (**21**) as the required integration over the involved finite areas is rather complicated. The emissivity coefficient of Siclanic was measured, by means of a Dornier Selectometer appliance (**22**). The emissivity of Graphite and Beryllium tiles was derived from a series of material tests performed by the JET Test Bed (**23**).

When there is no coolant in the i^{th} component (e.g. during Baking or Restart) then the second term on the RHS of Eq. (1) becomes zero and the general differential equation reduces to:

$$\sum W_i = m_i Cp_i \frac{dT_i}{dt} \tag{5}$$

As mentioned earlier, if the heat fluxes are known, the temperature of the i^{th} component can be easily found from Eqs. (1)-(3). The problem becomes more complicated when the temperatures of the components (and thus their associated heat fluxes), are not stable but change in a transient way. It is then necessary to determine the temperature variation of all the components involved, at the same time. Integration of the above set of equations for every component of concern then results in a system of at least 18 coupled non-linear differential equations.

7 MATHEMATICAL SOLUTION

Due to the complexity of solving the system of 18 differential equations analytically, a numerical technique was employed.

The set of equations is replaced by finite difference equations and is solved in a step by step explicit approach. The derivative $\frac{dT}{dt}$ can be approximated over a time step Δt as follows (**24**), (**25**):

$$\frac{dT}{dt} = \frac{T(t + \Delta t) - T(t)}{\Delta t} \tag{6}$$

Consequently, the problem domain (i.e., the time period of a transient) is discretized, and the values of the unknown dependent variables (temperature) are calculated only at a finite number of nodal points (i.e. the nodes are the two ends of every Δt period) instead of every point over the time domain. Note that the geometric complexity of the problem is incorporated via the view factors in Eq. (3). Discretizing Eqs. (1) and (2) yields the following algebraic expressions.

$$m_i\, c_{pi} \frac{T_i(t + \Delta t) - T_i(t)}{\Delta t} =$$

$$\pm \sum W_i - m\, C_p{}^{l} (T^{l}_{out} - T^{l}_{in}) \Big|_{\Delta t} \tag{7}$$

$$m\, C_p{}^{l} (T^{l}_{out} - T^{l}_{in}) \Big|_{\Delta t} = KA\, \Delta\theta_m \tag{8}$$

where,

$T_i(t)$, $T_i(t+\Delta t)$ = temperature of the i^{th} component at time, t, and time, $t+\Delta t$

T^{l}_{in}, T^{l}_{out} = fluid inlet and outlet temperature

Equations (1)-(5) are solved in a step by step approach. The code first calculates the steady state temperatures of the concerned components by putting $dT_i=0$ in Eq. (1), and solving Eq. (2) for T_i. The equilibrium temperatures are then the input for the transient analysis at time $t=0$. The explicitly calculated component temperature at time t then becomes the input value for the next time step integration, between t and $t+\Delta t$. Note that the time step, Δt must be small enough to ensure that numerical instabilities can be avoided. Typically 1200 time steps are required which takes less than 300 secs of CPU time on an PC with a 486 processor at 66 MHz.

8 MODEL VALIDATION

The experimental program had to be designed so that unnecessary risks would not be placed on the system, since simulating accident events can be extremely hazardous. Such considerations hold for almost every environment and this is perhaps why most of the safety studies of fusion reactors are not supported by experiments of real scale components e.g., (**26**), (**27**), (**28**).

Two types of experiments were carried out, (a) in a special test rig using a spare quadrant of the cryopump and (b) inside the JET vessel, involving minimum risks and the least delay on the availability of the machine. In addition real accidental events which occurred during operation of the JET machine have also been analysed, (**8**), (**29**).

The divertor cryopump is monitored by data acquisition software. Four PT100 temperature sensors (at inlet, outlet of LN flow, front and back panel) are included in the pump's instrumentation. The experimental data in this work are the records from these sensors. In addition, the JET Control and Data acquisition systems record continuously and simultaneously ~70,000 signals, among others the vessel temperature and pressure, the temperature on a number of tiles on the target plates, etc.

8.1 *Test Rig experiments.*

A spare quadrant of the cryopump was installed inside the test rig. The pressure in the test chamber was recorded by an MKS baratron transducer and two Leybold Heraeus gauges (one Pirani and one Penning). The temperature was measured by a set of 4 sensors attached to the LN panels, while the mass flow was recorded by a Parkinson Cowan type flowmeter, attached at the return Gaseous Nitrogen (GN) line. Finally, a set of pressure transducers and pressurised bottles of GN and deuterium were attached to a special port of the test rig.

The supply of cryogens to the spare quadrant was performed in a fully automatic fashion and all measurements were continuously recorded.

8.1.1 *Heat transfer modes*

The dominant heat transfer modes, under different vacuum conditions, were determined by examining the LN consumption required to keep all temperature sensors of the rig below 100K. The LN consumption is proportionally related to the incident heat which in turn depends on the pressure. Figure 5 shows consumption versus rig pressure. It may be seen that for pressures less than 10^{-3} mbar the LN flow is constant. With pressures between 10^{-3} mbar and ~2 mbar the consumption depends almost linearly on the pressure and the dependence becomes non-linear above 2 mbar. These pressure regimes can be correlated to heat transfer modes as follows (**30**): For pressures lower than 10^{-3} mbar the dominant heat transfer mode is radiation. Between pressures of 10^{-3} and 2 mbar, molecular conduction and the transition to viscous flow occur. Finally for pressures higher than 2 mbar heat is transferred both by conduction and convection (viscous flow).

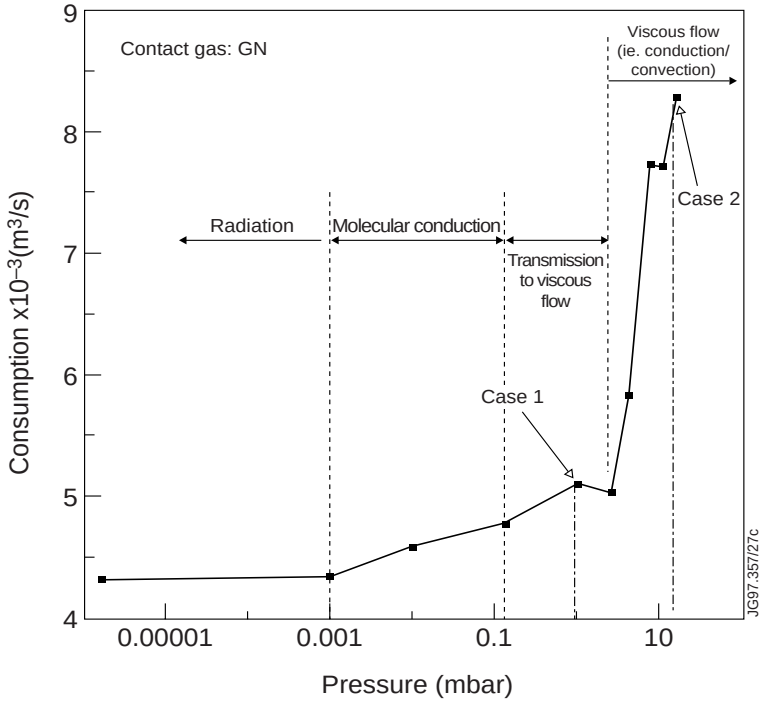

Figure 5. Recorded test rig pressure versus minimum liquid nitrogen consumption, needed to keep the spare quadrant at temperatures lower than 100 K.

Using the GrPr criterion (Grasshof Prandtl) for distinguishing conduction from convection in viscous flow (**31**), the model shows that when pressure is 1 mbar (Case 1 in Fig. 5) the heat transfer mechanism which prevails is conduction while for pressures of 15 mbar (Case 2 in Fig. 5) convection prevails (i.e., $GrPr>10^3$). Both of these predictions are in agreement with the conclusions based on the LN consumption.

8.1.2 *Radiation warm-up*

Figure 6 illustrates the situation when LN flow is stopped and the cryopump allowed to reach ambient temperature. A good vacuum is maintained throughout. The comparison between the measured and predicted temperature evolution for the front and back plates of the cryopump during the warm-up process are shown. The warm-up time constant is ~30,000 sec and was accurately predicted by the model. In addition the model and the experiment agree in the detailed time temperature evolution of the cryopump, though for times less than 20,000 seconds the temperature difference is underestimated by the model. It may be seen that the maximum global temperature gradient of the LN panels, ΔT, is ~30K (=30^{o}C), well below the 150^{o}C limit.

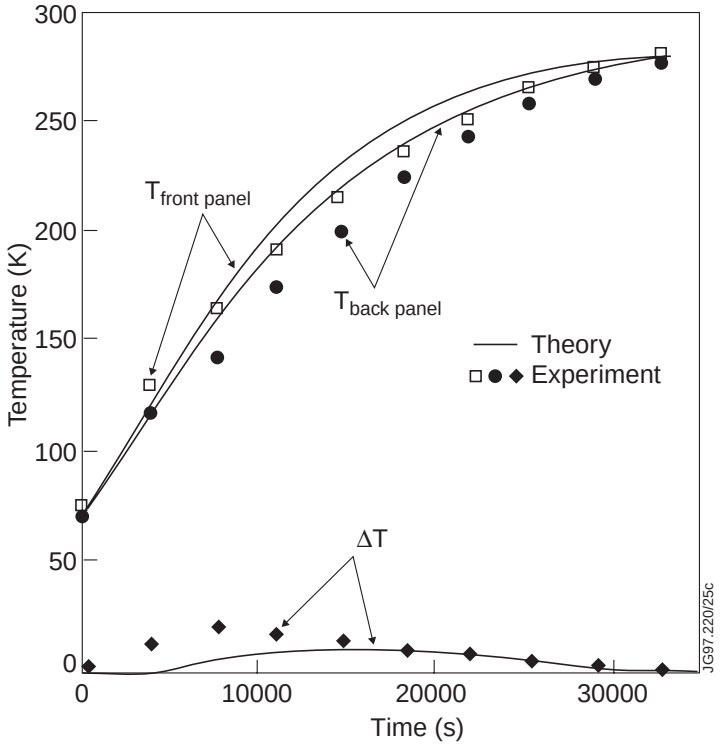

Figure 6. Comparison between experimental and predicted temperature evolution of the spare pump-quadrant, after loss of liquid nitrogen flow and good vacuum conditions in the test rig.

8.1.3 *Warm-up with loss of vacuum*

The situation of loss of vacuum is examined by introducing deuterium and nitrogen (typical in-vessel gases) as contact gases at different pressures into the test rig. Before analysing experiments with contact gases it is important to check whether condensation mechanisms are significant. In the experiments which follow, only LN was supplied to the spare quadrant, while the helium panels were kept empty. Deuterium condenses at temperatures much lower than 77K (this gas is pumped by LHe). Furthermore, at pressures of a few mbar, the condensation limit for gaseous nitrogen is about 60 K and thus it also cannot condense on the LN panels, which operate at 77K.

The warm-up curves of the spare quadrant following stoppage of LN with 1 mbar deuterium inside the ambient test rig are illustrated in Fig. 7. It may be seen that the time constant is somewhat reduced due to higher heat transfer fluxes, as are the ΔTs. (Compare with Fig. 6.) Both of these trends are well predicted by the model.

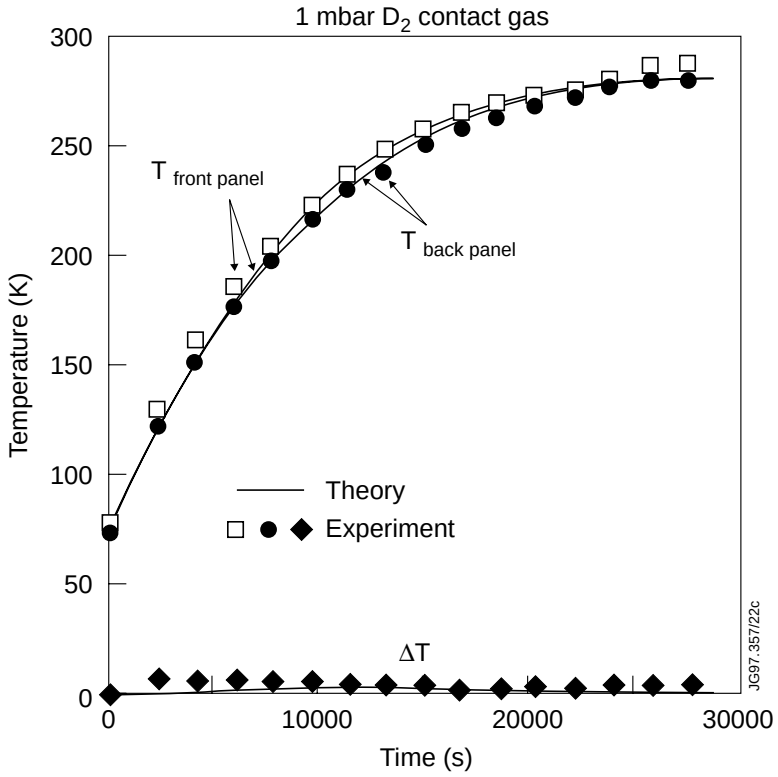

Figure 7. Comparison between experimental and predicted temperature evolution of the spare pump-quadrant, after loss of liquid nitrogen flow and bad vacuum conditions (1 mbar Deuterium) in the test rig.

The results for 15 mbar Nitrogen inside the test rig are shown in Fig. 8. Again the agreement between the theory and the experiment is satisfactory.

8.1.4 *Forced warm-ups*

Whenever there is a need for a machine shut-down or an in-vessel intervention, the cryogenic flow is stopped intentionally. The warm-up time of the cryopump can be shortened by introducing ambient GN in its circuit, soon after the stoppage of the LN. This action is referred to as forced warm up and assists in reducing the overall down time (thus increasing the availability of the machine). Figure 9 gives the results of a forced warm-up of the spare quadrant with 19 gr/sec GN under a good vacuum. The warm-up period is now much shorter (~5000 sec) compared to the previous experiments, and the maximum global ΔTs are again very low. The agreement between the predictions and measurements is again good.

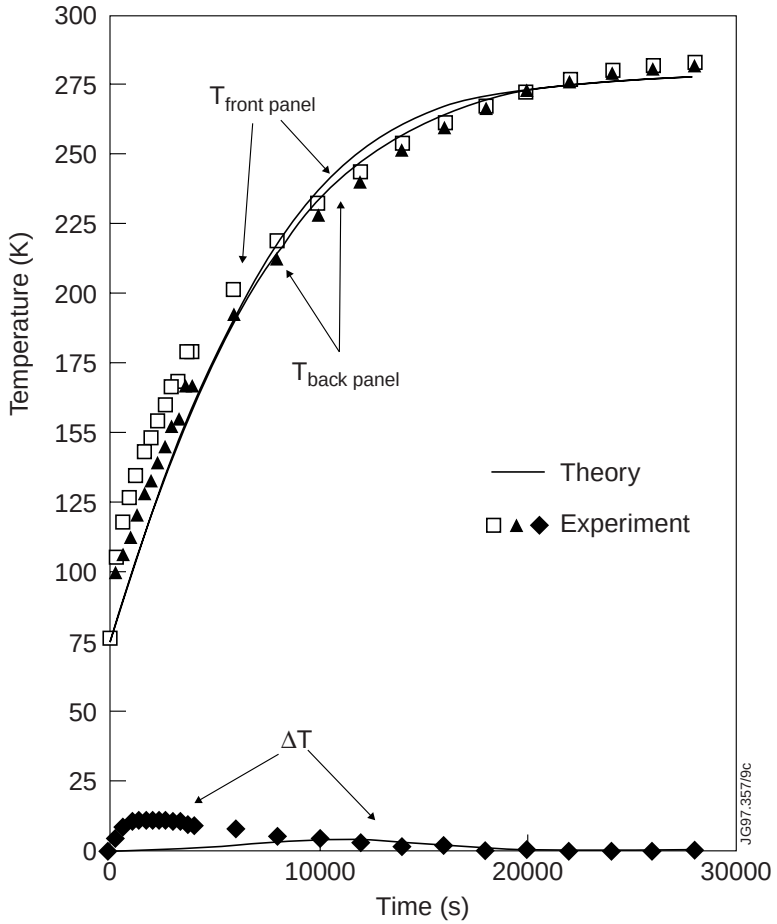

Figure 8. Comparison between experimental and predicted temperature evolution of the spare pump-quadrant, after loss of liquid nitrogen flow and bad vacuum conditions (15 mbar Nitrogen) in the test rig.

For further validation of the model, the measured and predicted temperature of the GN at the outlet during the warm-up experiment under good vacuum are also compared in Fig. 10. The good agreement may be seen in both.

The case of a forced warm-up but under controlled loss of vacuum conditions (insertion of 15 mbar GN in the rig) is examined in Fig. 11. The transient time period is the shortest observed during the experimental campaign (~4000 sec) due to the high levels of incident heat on the pump. The maximum global ΔTs are still very moderate.

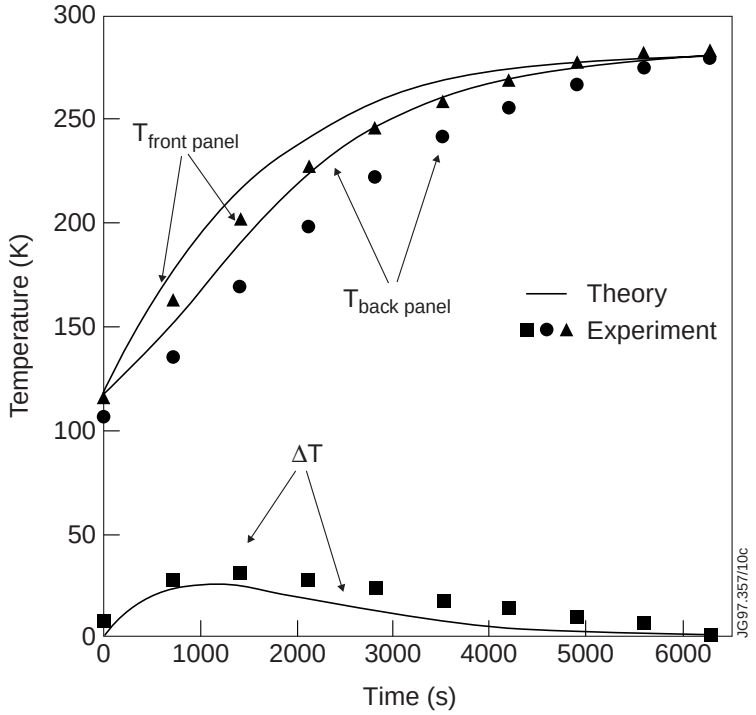

Figure 9. Comparison between experimental and predicted temperature evolution of the spare pump-quadrant, during a forced warm-up, with 19 gr/sec GN in the liquid nitrogen pipework and good vacuum conditions in the test rig.

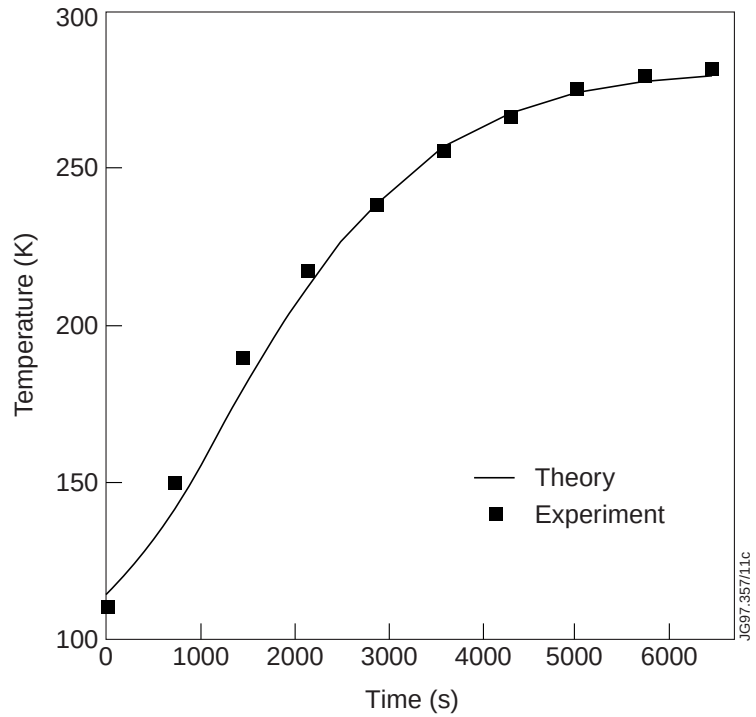

Figure 10. Comparison between theoretical and experimental GN exit temperature during the forced warm-up under good vacuum.

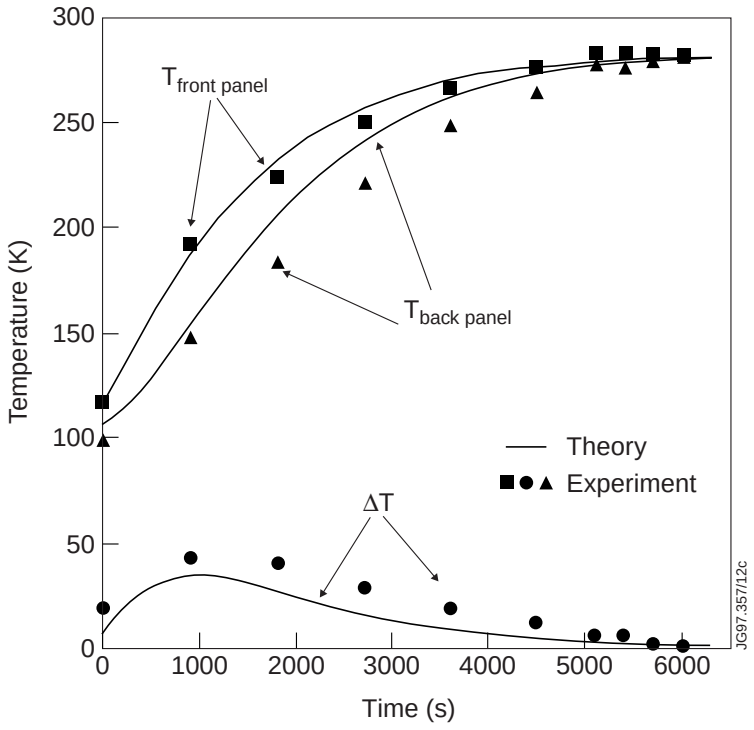

Figure 11. Correlation between experimental and predicted temperature evolution of the spare pump-quadrant, during a forced warm-up, with 19 gr/sec GN in the liquid nitrogen pipework and bad vacuum conditions in the test rig (15 mbar nitrogen)

8.2 In-vessel experiments

Following the first cool-down of the cryopump with LN, the latter was intentionally stopped four hours after reaching equilibrium, with water running through the water cooled components. The vessel temperature was at ~80^{o}C while the torus vacuum was good. The temperature histories of the cryopump under the radiation warm-up, as predicted by the model are compared with the experimental data in Fig. 12. The good agreement is noted.

A loss of water flow event occurred while operating with the MK2 divertor and the cryopump was forced to undergo a warm up (i.e. LN flow was stopped). The warm-up, with cooling water flowing in the MK2 target plates, good torus vacuum, baffles without water and vessel at 320^{o}C is illustrated in Fig. 13, together with the relevant recordings. Although the model predicted higher initial warm-up rates the total transient time constant (~33000 sec) and the maximum ΔTs are adequately simulated. The reason for the difference at the beginning of the transient may be attributed to the localised loss of water flow in the baffles (which took place in one or two octants at first), and consequently the boundary conditions, in this case, were difficult to define accurately.

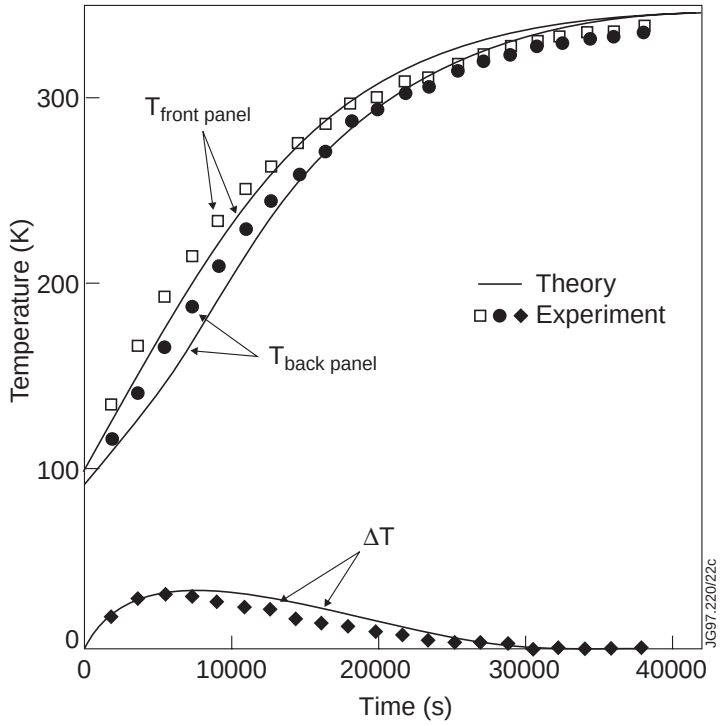

Figure 12. Comparison between the predicted and measured uncontrolled warm-up of the in-vessel cryopump, with good torus vacuum, vessel at 80°C and water flowing in the system.

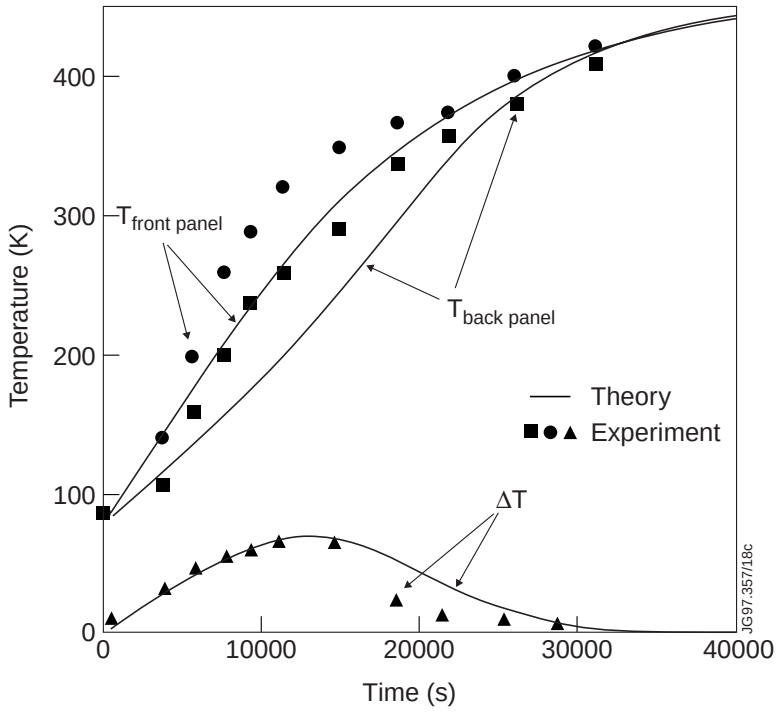

Figure 13. Real accident simulation in the MK2 Divertor, with loss of liquid nitrogen flow in the cryopump, no water in the baffles, vessel at 320°C and good torus vacuum.

9 SAFETY ANALYSES OF THE DIVERTOR CRYOPUMP

Following successful validation of the model, an extensive investigation of the cryopump behaviour was undertaken. Since describing all the cases examined is beyond the scope of this

work, a selected set of the most significant results will be presented.

9.1 Accident analyses during Baking

During baking there is no water flowing in the water-cooled components and only the coils are kept cold. The most severe conditions for the cryopump are when the vessel temperature is at its highest value, i.e., 350°C. High vessel temperatures result in high thermal fluxes and maximum *ΔTs* in the cryopump. If the cryopump can cope with the high heat fluxes under these conditions then the risk will be much less at lower vessel temperatures.

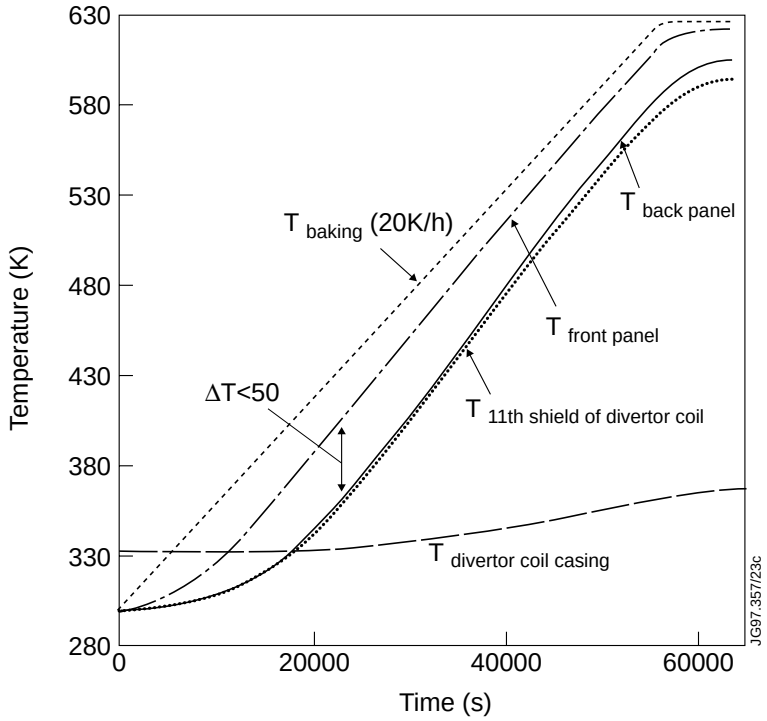

Figure 14. Temperature evolution of the divertor cryopump and its associated components during baking up to 350°C (at a rate of 20K/h). All components except the divertor coil are empty of coolants.

It was found that during baking with the vessel at 350°C and under good torus vacuum, the developed global *ΔT*s on the cryopump are moderate (< 50°C), much lower than the limit of 150°C as can be seen from Fig. 14. If, in addition to the above, there is loss of vacuum, by an air leak at 1 bar the maximum *ΔT*s reach a value of ~100°C, ensuring that there is again no operational risk under these conditions

9.2 Accident analyses during Restart

In the Restart mode, the water- cooled components are again empty of coolants and the vessel temperature is usually low. An analysis was carried out to determine under what conditions the cryopump can be safely fed with cryogens, (i.e. without exceeding the limit of 150°C). The answer to this question was based on the following considerations:

Cool-down ΔTs were ignored, since simulation of cool down processes are not included. Hence it was assumed that the cryopump was cooled down safely. With cryogens flowing, there is still the possibility of a loss of cryogen flow, (i.e., uncontrolled warm-up) prior to water introduction in the water-cooled components, or after partial introduction to one system only.

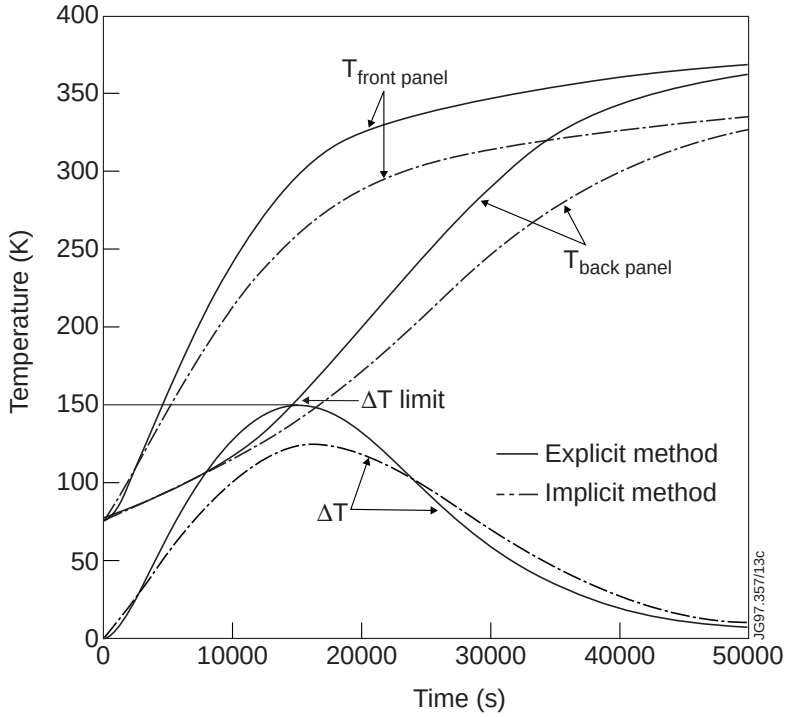

Figure 15. A conservative simulation of a general and simultaneous loss of coolant flow event (i.e., cryogens, water), under good vacuum conditions, and the vessel at 100°C.

Figure 15 displays a conservative (in terms of incident heat flux) simulation of a loss of cryogen flow scenario, under good torus vacuum, no water in the relevant in-vessel circuits and the vacuum vessel at 100°C. It appears that the resultant thermal gradients are close to the limit of 150°C. Therefore the model dictates that during restart, the cryopump cannot be fed by cryogens until the vessel temperature falls below 100°C. (However, it should be pointed out that this particular analysis had incorporated conservative emissivity values in order to accommodate an enhanced safety margin.)

9.3 Accident analyses during Normal Operation

9.3.1 *Simultaneous loss of coolant flow*

In Fig. 16(a) the temperature evolution of the cryopump and baffles is shown with loss of coolant flow in these components, the vessel at 350°C and there an air leak at 1 bar. Again the maximum ΔT is lower than 150°C.

The results under the similar conditions, but with water running in the water cooled components, and the vessel at 20°C is shown in Fig. 16(b). The maximum ΔTs are below 150°C, and, as expected, are lower than the previous case, because the cryopump is now protected by the surrounding water cooled components.

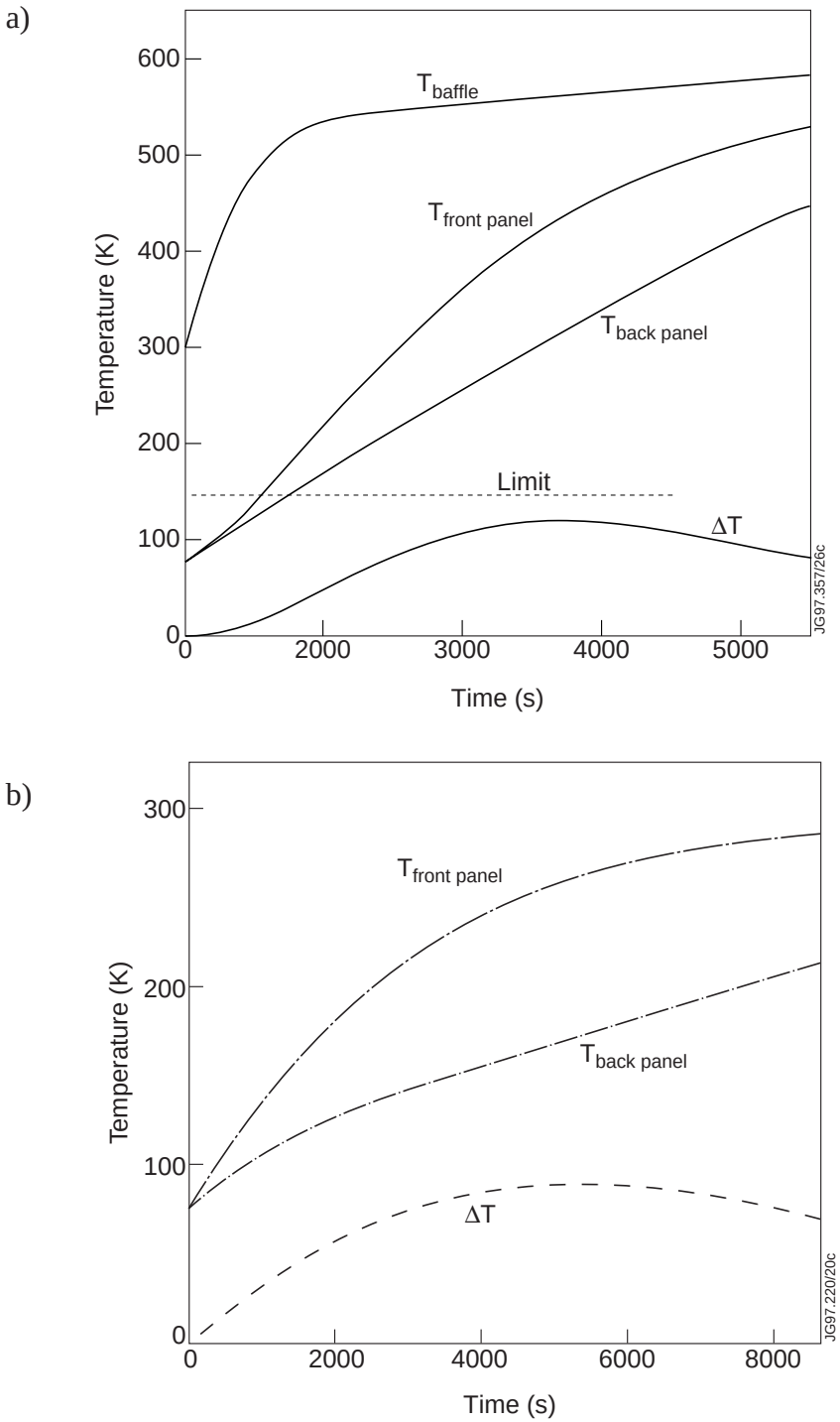

Figure 16. (a) Simulation of a simultaneous loss of coolant flow in the cryopump and the water cooled baffles, with the vessel at 350°C and an air leak of 1 bar in the JET torus;

(b) As in (a) but with water flowing in the relevant components and vessel at 20°C.

9.3.2 *Effect of Draining following a Loss of water flow*

A loss-of-water-flow incident inside the vessel, during normal operation, with the vessel at 350^{o}C, and good vacuum, results in a slow transient increase in temperature of the relevant water cooled component. Even if the water cooled components are drained, there is still a possibility that their temperature may exceed 100^{o}C. Following such a development and should there be an additional loss or stoppage of LN supply, subsequent introduction of cryogens may be unsafe, as discussed in Section 9.2.

Detailed analysis showed that within 2 hours of the loss of water flow, the relevant components (i.e., baffles and target plates) reach 100^{o}C. This indicates that if water flow cannot be reinstated within 2 hours, then the cryopump should be drained of cryogens, in order to prevent the development of high stresses.

10 DISCUSSION

The results of the analyses may be summarised as follows: the cryopump can be operated (or baked) with vessel temperatures up to 350^{o}C without exceeding the temperature gradient limit of $\Delta T = 150^{o}C$, in almost all possible abnormal scenarios (loss of water, cryogen flow, vacuum, combinations). However, the cryopump cannot be fed with cryogens if the vessel temperature is higher than 100^{o}C during the restart mode, and it should be drained if there is loss of water flow, for more than 2 hours with the vessel hot and under good torus vacuum. Loss of vacuum in the latter case is of no risk. The results presented here are for the MK1 divertor. The results for the MK2 Divertor (Fig. 4b) are almost identical. This is because the operating conditions, view factors and emissivities are almost the same for both divertors.

The basic characteristic of the developed model is its flexibility, ability to incorporate alterations in geometry, and capability of estimating the transient thermal behaviour of a complex system of components. The temperatures, or temperature differences (ΔTs) calculated by the code are global values since only average temperatures are dealt with. Estimates of local temperature changes, i.e. variation along a component, have also been made (**8**). For the cases examined the local ΔT's are at least an order of magnitude less than the global ΔT's and thus can be ignored.

The accuracy of the results depends on the size of the chosen time step (**24**), (**25**), (**32**). Therefore, the desired accuracy can be easily achieved by choosing a small time step, with regard to the duration of the examined transient. The optimum value of the time step was chosen against a converged solution.

The developed model has been extensively validated through experiments on real scale components. An entirely automatic safety system based on the findings of the present model, has been implemented in the JET device. On a practical level the adequacy of the design of the cryopump and the efficiency of the safety actions proposed have been proven by two years of safe operation within the JET Tokamak.

11 CONCLUSIONS

A model has been developed from first principles to perform steady state and transient analyses with regard to hypothetical accident scenarios involving the JET in-vessel cryopump and its associated components.

A series of experiments both inside the torus and in a test chamber simulating various abnormal cases were successfully analysed by the code. After numerous simulations under diverse boundary conditions and abnormal scenarios it was shown that the cryopump can withstand all envisaged abnormal scenarios without introducing excessive stresses.

In Part II of this work (**29**) the behaviour of a similar cryogenic component, the JET LHCD pump will be analysed. Similar analyses concerning freeze-up or boiling risks of in-vessel water cooled components can be found in (**8**), (**33**).

ACKNOWLEDGEMENTS

The authors wish to acknowledge the vital contribution of the JET Cryogenics Group in designing the experiments and allowing access to their facilities and control rooms. Special thanks also to Dr D Stork, Dr W Obert, Dr H Van der Beken, and Dr P Karditsas for comments and discussions and to the JET Graphics Group for editing figures and diagrams.

REFERENCES

1 **The Commission of the European Communities**: The European Programme for the Controlled Thermonuclear fusion, *Report EUR 6269 GR*, 1983.

2 **Kadomtsev, B. B.** *Tokamak Plasma; A Complex Physical System*, 1992, **Chpt**. **3**, 9-13 (IOP Publishing Ltd. Philadelphia, US).

3 **Bertolini, E. for the JET Team**. The JET Project: Progress Toward a Tokamak Thermonuclear Reactor, *Journal of Power Engineering*, 1993, **3**, 105-140.

4 **Bertolini, E. for the JET Team**. JET with a Pumped Divertor: design, construction, commissioning and first operation, *Fusion Engineering & Design*, 1995, **30,** 53-66 (North Holland, Amsterdam).

5 **The JET Team (presented by Tanga, A.).** First Results with the Modified JET. Journal of *Plasma Physics & Controlled Fusion*, 1994, **36**, 39-54 (Inst. of Physics Publishing, UK).

6 **The JET Team (prsented by Keilhacker, M.).** JET Results with the New Pumped Divertor and Implications for ITER, Journal of *Plasma Physics & Controlled Fusion*, 1995, **37**, 3-18 (Inst. of Physics Publishing, UK).

7 **Papastergiou, S., Obert, W. and Thompson, E.** Materials Selection, Qualification and Manufacturing of the In-Vessel Divertor Cryopump for JET, Proc. On *Advances in Cryogenic Engineering*, 1993, **40B**, 1429-1436, (Plenum Press, New York).

8 **Ageladarakis, P.** Aspects of Operational Safety & Mechanical Integrity of the Cryopump System in the JET Fusion Tokamak, *PhD Thesis* 1996, Imperial College, London.

9 **Starkey, D.E. and the JET Stress Office.** *JET Memorandum*, February 1994.

10 **Saibene, G., et al.** Review of Vacuum Vessel Conditioning Procedures at JET and their Impact on Plasma Operation, Journal of *Nuclear Materials*, 1995, **220,** 617-622 (Elsevier Science Publishing, Amsterdam).

11 **Baker, C., et al.** STARFIRE - A Commercial Tokamak Fusion Power Plant Study, *Argonne Laboratory, ANL/FPP-80-1*, September 1980.

12 **ESECOM.** The Senior Committee on Environmental, Safety and Economic Aspects of Magnetic Fusion Energy, *ESECOM-Final Report, U.S. DOE*, 1987.

13 **Obert, W., et al.** JET Pumped Divertor Cryopump. Proc. of 16th Symposium on *Fusion Technology*, 1990, **16-1**, 488-492, (Elsevier Science Publishing, Amsterdam).

14 **Sanazzaro, G., Barabaschi, P.** Stress analysis and loads in the divertor cryopump and water cooled baffles during a plasma disruption, *JET Memorandum*, July 1990.

15 **Papastergiou, S and Ageladarakis, P.** Effects of High Frequency Disruptions on the JET Divertor Cryopump including Potential JET Toroidal Field Upgrades, 19th Symposium on *Fusion Technology*, Lisbon, Portugal, September 1996.

16 **Ying, A.Y., Raffray, A.R., and Abdou, M.** Benefits of Natural Convection in Solid Breeder Blankets with Poloidal Coolant Channels under LOFA Conditions, *Fusion Engineering and Design*, 1991, **17**, 313-319.

17 Ying, A.Y., Raffray, A.R., and Abdou, M. LOFA Analysis for US ITER Solid Breeder Blanket, *Fusion Technology*, 1991, **19**, 1481-1486.

18 Gorbis, Z. R., et al. LOCA Study for a Helium-Cooled Solid Breeder Design for ITER, *Fusion Technology*, 1989, **15**, 821-826.

19 Lewis, E. E. *Nuclear Power Reactor Safety*, 1977, (John Wiley & Sons, Inc.).

20 Tong, L. S. and Weisman, J. Thermal analysis of Pressurised Water Reactor, 2nd edition, *American Nuclear Society*, Illinois 1979,134-141.

21 Siegel, R., Howell, J.R. *Thermal Radiation Heat Transfer*, 1983, **Chpt 7** , 202-210, (Hemisphere Publishing Corp., New York).

22 Perinic, G., Scherber, W., Schulz, K. A Portable Instrument for measuring emissivities, Proc. on *Advances in Cryogenic Engineering*, 1996, **41**, 1851-1855, (Plenum Press , New York).

23 Falter, H. D., et al. High Heat Flux Exposure Tests on 10 mm Beryllium Tiles Brazed to an Actively Cooled Vapotron made from CuCrZr, *JET Report, JET-R(96)02*, 1996.

24 Minkowycz, W.J., Sparrow, E.M., Schneider, G.E., Plechter, R.H. *Handbook of Numerical Heat Transfer,* 1988,**Chpt 1**, 40-43, (John Wiley & Sons Inc. New York).

25 Hamming, R. W. *Numerical Methods for Scientists and Engineers*, 1962, **Chpt 14**, 185-186, (McGraw Hill Book Company Inc, London).

26 Rocco, P., et al. Safety Analysis of a Loss of Coolant Accident in a Breeding Blanket for Experimental Fusion Reactors, *Fusion Technology*, 1985, **8**, 1415-1420.

27 Mazille, F., and Djerassi, H. Analysis of LOCA/LOFA Risks for the Water Cooled First Wall of the NET Type Fusion Reactor, 15th Symposium on *Fusion Technology*, 1988, **15-2**, 1740-1745, (Elsevier Science Publishing, Amsterdam).

28 Ebert, E., and Raeder, J. LOCA, LOFA and LOVA analyses pertaining to NET/ITER safety design guidance, *Fusion Engineering & Design*, 1991, **17**, 307-312, (Elsevier Science Publishers, Amsterdam).

29 P Ageladarakis, S Papastergiou, N P O'Dowd and G A Webster, Theoretical and Experimental Simulation of Accident Scenarios of the JET Cryogenic Components Part II: The LHCD Cryopump, submitted for publication.

30 Obert, W. Private Communication, 1994.

31 Verein Deutcher Ingenieure-VDI. VDI-Warmeatlas,Gesellshaft Verfahrenstechnik Chemieingieurweaen *(GVC)*, Dusseldorf, 1988.

32 Patangar, S.V. *Numerical Heat Transfer and Fluid Flow***,** 1980, (Hemisphere Publishing Corporation, New York).

33 Ageladarakis, P., Papastergiou, S., Stork, D., and Van Der Beken, H. The Model and Experimental Basis for the Design Parameters of The JET Divertor Cryopump Protection System Including Variations in Divertor Geometry and First Wall Materials, 19th Symposium on *Fusion Technology*, Lisbon, Portugal, September 1996.